



Hysteresis of idealized, instability-prone outlet glaciers under variation of pinning-point buttressing

Johannes Feldmann¹, Anders Levermann^{1,2,3}, and Ricarda Winkelmann^{1,2}

¹Potsdam Institute for Climate Impact Research (PIK), Potsdam, Germany

²Institute of Physics, University of Potsdam, Potsdam, Germany

³LDEO, Columbia University, New York, USA

Correspondence: Johannes Feldmann (johannes.feldmann@pik-potsdam.de)

Abstract. Ice rises or ice rumples act as ice-shelf pinning points that can have an important role in regulating the ice discharge of marine outlet glaciers. As an example, the observed recent gradual ungrounding of the ice shelf of West Antarctica's Thwaites Glacier from its last pinning points likely diminished the buttressing effect of the ice shelf and thus contributed to the destabilization of the outlet. Here we use an idealized experimental setting to simulate the response of an Antarctic-type, instability-prone marine outlet glacier to a successive ungrounding of its ice shelf from a topographic high and a subsequent re-grounding. We show that the glacier retreat down the landward down-sloping (retrograde) bed, induced by the loss in pinning-point buttressing, can be unstable and irreversible given a relatively deep subglacial bed depression. In this case, glacier retreat and re-advance show a hysteretic behavior and if the bed depression is sufficiently deep, the glacier does not recover from but remains locked in its collapsed state. Conversely, reversibility requires a sufficiently shallow bed depression. Based on a simple flux balance analysis, we argue that the combination of a deep bed depression and limited ice-shelf buttressing hampers grounding-line re-advance due to the dominant and highly non-linear influence of the bed depth on the ice discharge across the grounding line. We conclude that outlets that rest on a deep bed depression and are weakly buttressed, such as Thwaites Glacier, are more susceptible to abrupt and irreversible retreat than stronger buttressed glaciers on more moderate retrograde slope, such as Pine Island Glacier. In particular, our results suggest that the wide and deep marine bed depression in the interior of Thwaites Glacier's drainage basin might promote potential future unstable retreat and also represent a strong limitation for a possible re-advance of the glacier in case it would collapse.

1 Introduction

Where the floating ice shelves ground on locally elevated seabed, ice rises or ice rumples form. Such ice-shelf pinning points are scattered along major parts of the Antarctic coast (Matsuoka et al., 2015, Fig. 3). Many of them provide enough basal drag to exert a buttressing force on the upstream grounded tributaries that feed the ice shelves (pinning-point induced buttressing), and thus act as a regulator of outlet-glacier ice discharge (Goldberg et al., 2009; Gagliardini et al., 2010; Favier et al., 2012; Berger et al., 2016; Reese et al., 2018). For instance, the ungrounding of East Antarctica's Brunt Ice Shelf from a pinning point in the course of a calving event in the early 1970s has been suggested to have led to a quasi-instantaneous twofold increase in the ice shelf's flow speed (Gudmundsson et al., 2017). Cray Ice Rise of the Ross Ice Shelf has been estimated to exert a resistance



25 that accounts for about half of the buttressing forces acting on the upstream Whillans Ice Stream (Macayeal et al., 1987).
In-depth numerical modeling studies have investigated, e.g., the speed-up of Larsen C Ice Shelf in response to a reduction in
pinning-point buttressing (Borstad et al., 2013), the effect of pinning points on marine outlet glacier stability and grounding
line (GL) dynamics in the region between Lazarev and Roi Baudouin ice shelves (Favier et al., 2016), the influence of surface
30 accumulation rate and ocean perturbations on ice-rise divide migration at Ekström Ice Shelf (Schannwell et al., 2020) or the
hysteretic evolution of ice rises and rumples under variations of sea level and basal friction in idealized simulations (Henry
et al., 2022). Evidence from paleo records suggests that ice-rise formation generally played an important role in Antarctica's
glacial history, interfering with the cyclic retreat and advance of the ice sheet (Matsuoka et al., 2015).

While pinning points have the potential to restrain upstream ice flow substantially, ice-shelf buttressing can also emerge
from horizontal shearing at the lateral margins of an ice shelf, if it is confined by slowly moving grounded ice or the bed
35 topography (confinement-induced buttressing; Dupont and Alley, 2005; Gudmundsson et al., 2019). In Antarctica, many ice
shelves provide a combination of pinning-point induced buttressing and confinement-induced buttressing to the upstream ice
flow. Examples range from relatively small, narrow ice shelves with few and small pinning points, like West Antarctica's Pine
Island Ice Shelf (Arndt et al., 2018) to the two largest and widest of the ice sheet that incorporate numerous and partly very
large pinning points, i.e., Ross and Filchner-Ronne ice shelves (Matsuoka et al., 2015; Still et al., 2019).

40 Observations over the last two decades indicate that strong basal melting has thinned the ice shelves of West Antarctica's
Amundsen Sea sector including the ice shelves of Pine Island and Thwaites glaciers (Paolo et al., 2015; Shepherd et al., 2018;
De Rydt et al., 2021; Joughin et al., 2021). The associated buttressing reduction resulted in enhanced ice discharge, speed-up
and GL retreat of the two outlets (Konrad et al., 2018; Milillo et al., 2019; De Rydt et al., 2021; Rignot et al., 2022). Part of this
buttressing loss was due to the ice shelves' un-grounding from several of their pinning points in the course of their thinning
45 (Tinto and Bell, 2011; Arndt et al., 2018). The ice shelf of Thwaites Glacier continues to gradually lose contact to its last
remaining pinning points (MacGregor et al., 2012; Rignot et al., 2014; Alley et al., 2021; Benn et al., 2022) and could unpin
completely in less than a decade (Wild et al., 2022). This might further decrease pinning-point buttressing and contribute to the
imbalance of the glacier also in the future (Bett et al., 2023), although to a possibly limited extent (Gudmundsson et al., 2023).
The pinning points of the neighboring retreating Smith and Kohler Glaciers are also observed to be vanishing (Rignot et al.,
50 2014; Milillo et al., 2022).

The above mentioned West Antarctic glaciers are principally prone to the so-called marine ice-sheet instability (MISI;
Mercer, 1978; Schoof, 2007; Pattyn, 2018; Sergienko, 2022) as they are resting on bed well below sea level that is generally
sloping down in landward direction (retrograde bed slope; Morlighem et al., 2020). An ongoing destabilization of these outlets
might lead to a disintegration of the West Antarctic Ice Sheet in the long term with the potential to raise global mean sea level
55 by several meters (Bamber et al., 2009; Feldmann and Levermann, 2015; Ritz et al., 2015; Reese et al., 2023). Among various
processes, mechanisms and feedbacks potentially affecting ice-sheet (de)stabilization (e.g., Brondex et al., 2017; Pegler, 2018;
Sergienko, 2022; Christie et al., 2023), the influence of pinning points has been suggested to play a decisive role regarding



the timing, extent and even possible reversal of MISI-type retreat (Goldberg et al., 2009; Matsuoka et al., 2015; Favier et al., 2016).

60 Here we take a conceptual approach to investigate the response of a MISI-prone outlet glacier system to progressive pinning-point ungrounding and re-grounding in idealized numerical simulations. Altering the buttressing strength of the pinning point that stabilizes the outlet glacier on retrograde bed, we show how the depth of the subglacial bed depression can affect (ir)reversibility of glacier retreat and advance in an ensemble of hysteresis experiments. To explain the qualitatively very different responses of the simulated similar ice-sheet-shelf systems, we provide a simple analysis of the steady-state ice flux
65 balance at the GL based on Schoof (2007), quantifying the non-linear influence of both the local bed depth and the pinning-point buttressing strength on ice discharge across the GL. The numerical model and the experimental design are outlined in Sect. 2. The results are presented in Sect. 3 and discussed in Sect. 4 before the conclusions are drawn in Sect. 5.

2 Methods

2.1 Numerical model

70 We use the open-source Parallel Ice Sheet Model (PISM; Bueler and Brown, 2009; Winkelmann et al., 2011), which applies a superposition of the shallow-ice approximation (SIA; Morland, 1987) and the shallow-shelf approximation (SSA; Hutter, 1983) of the Stokes stress balance (Greve and Blatter, 2009). In particular, the SSA allows for stress transmission across the GL and thus accounts for the buttressing effect of ice shelves that are laterally confined (Gudmundsson et al., 2012; Fürst et al., 2016; Reese et al., 2018) and/or in contact with a pinning point (Favier et al., 2012; Matsuoka et al., 2015; Wild et al., 2022).
75 The model applies a linear interpolation of the freely evolving GL and accordingly interpolated basal friction (Feldmann et al., 2014). GL migration has been evaluated in the model intercomparison exercises MISMIP3d (Pattyn et al., 2013; Feldmann et al., 2014) and MISMIP+ (Asay-Davis et al., 2016; Cornford et al., 2020). To improve the approximation of driving stress across the GL, the surface gradient is calculated using centered differences of the ice thickness across the GL (Reese et al., 2020).

80 2.2 Setup and experimental design

Our topographic setup is designed to model a MISI-prone outlet glacier that is stabilized by a pinning point in the center of the glacier's ice shelf (Fig. 1). For this purpose we prescribe a modified version of the channel-type MISMIP+ bed topography, $B_{CH}(x, y)$, as used in Feldmann and Levermann (2023, Appendix C) and superpose a submarine topographic high, $B_{TH}(x, y)$, in the ice-shelf region of the setup such that the resulting bed topography applied in our simulation is given by

$$85 \quad B(x, y) = B_{CH}(x, y) + B_{TH}(x, y). \quad (1)$$

The geometry of the Gaussian-shaped topographic high is adopted from Favier and Pattyn (2015) and has the form

$$B_{TH}(x, y) = H_{TH} \cdot \exp\left(\frac{-(x - x_{TH})^2 - (y - y_{TH})^2}{2 \cdot (15 \text{ km})^2}\right). \quad (2)$$



Here, H_{TH} denotes the height of the topographic high relative to the local elevation of the bed trough, $B_{CH}(x_{TH}, y_{TH})$, i.e.,

$$H_{TH} = -D_{TH} - B_{CH}(x_{TH}, y_{TH}), \quad (3)$$

90 where D_{TH} is the depth of the tip of the topographic high below sea level (Fig. 1b), which is varied in 20-m steps in the course of the hysteresis experiments. We use three versions of $B_{CH}(x, y)$ which differ in the depth of the bed depression D_{BD} below sea level (Fig. 1b). These three versions are termed "shallow" ($D_{BD} = 675$ m), "moderate" ($D_{BD} = 750$ m) and "deep" ($D_{BD} = 900$ m) in the following (Table 1). For each of these three topographies we place the topographic high at three different distances ($x_{TH} = 500, 600$ and 650 km) away from the ice divide, while in the y -dimension the topographic high is always
95 located at the centerline of the setup ($y_{TH} = 0$; Fig. 1a). This makes a total of nine distinct hysteresis experiments. Note that the shape of the bed topography is qualitatively the same in all experiments (Fig. 1b): along the setup centerline, the bed elevation drops from an inland sill into an overdeepening (deepest point of the bed depression at $x = 200$ km) and increases toward a coastal sill further upstream (highest point at $x = 500$ km) on which the topographic high is located.

For each hysteresis experiment, consisting of a series of steady-state simulations, the ice-sheet-shelf system is first spun up,
100 starting from a domain-wide layer of ice of 2000 m thickness. In this initial experiment the elevation of the topographic high is chosen such that the central GL position of the simulated outlet glacier stabilizes 1) on the coastal sill (around $x = 500$ km), i.e., close to the onset of the retrograde slope section (Fig. 2) and 2) upstream of the topographic high such that an ice-shelf pinning point emerges that is clearly distinct from the main GL of the outlet (except for the experiments in which the topographic high is located on the coastal sill; see Figs. 2g-i). The initial state is then perturbed by a 20-m lowering of the topographic-high elevation. The simulation is run until the glacier has reached a new equilibrium, i.e., until changes in the glacier volume have become negligible and the GL is in steady state again (Fig. S1). Starting from the new equilibrium, again the topographic-high elevation is lowered by 20 m and the system is run into steady state. These perturbation experiments are carried out
105 subsequently until the outlet's ice shelf has detached from the topographic high. The perturbation is then reversed, i.e., the unpinned equilibrium state is now perturbed by a 20-m increase of the topographic-high elevation. The step-wise increase in topographic-high elevation after each equilibration is continued until the original topographic-high elevation is reached. The step-wise forcing and the time evolution of the response of the glacier's centerline GL position throughout a complete series of subsequent steady-state experiments is exemplarily shown in Fig. S1 for each of the three different bed-depression depth. The incremental change in topographic-high elevation realizes a gradual reduction/increase in pinning-point induced ice-shelf buttressing in a synthetic but minimal-invasive manner, i.e., without directly changing the thickness, extent or softness of the
115 ice shelf (see discussion).

All experiments apply the same surface accumulation rate and ice softness, which are constant in space and time (see Table 1 for more parameters). Basal melting is set to zero. Basal friction is calculated according to a Weertman-type power law (Cornford et al., 2020, Eq. 3). The simulations are carried out on a regular horizontal grid of 2 km resolution, which has been shown to be suitable for accurately modeling fast ice dynamics in a previous study (Feldmann and Levermann, 2023). We
120 will refer to the experiments described above as laterally confined simulations throughout the remainder of the text, the results



of which are presented in Sect. 3.1. Based on these experiments we conduct a small set of additional simulations for which we removed the lateral confinement of the prescribed bed topography. These laterally unconfined simulations are detailed in Sect. 3.2.

3 Results

125 3.1 Laterally confined simulations

The general response of the simulated outlet glaciers to each incremental topographic-high lowering is characterized by a retreat of the GL due to the reduced buttressing effect of the pinning point (red curves in Fig. 3). Conversely, the subsequent step-wise elevation of the topographic high leads to GL re-advance due to the increase in pinning-point buttressing (blue curves in Fig. 3). Regarding the complete cycle of topographic-high lowering and subsequent raising we identify three qualitatively
130 different types of glacier response:

1. **Reversible behavior:** regardless of whether the glacier is retreating or regrowing, for a given topographic-high elevation the steady-state GL position is approximately the same. In the hysteresis diagram the path of the steady-state positions of the re-advancing GL is approximately the same as the path of the previously retreating GL (compare blue and red curves in Fig. 3a).
- 135 2. **Hysteretic behavior:** the regrowing glacier reverts to its original (initial) state but the steady-state GL positions depend on the history of glacier evolution. In other words, after large-scale retreat, the GL of the regrowing glacier requires a higher topographic-high elevation (more pinning-point buttressing) to re-advance towards its original position. This hysteresis gap between the path of GL retreat and the path of GL re-advance, ΔD_{TH} , is highlighted in Fig. 3b.
3. **Lock-in behavior:** the regrowing glacier does not revert to its original state. After ice-shelf re-grounding on the topographic high the GL advances only marginally and remains situated on the inland sill near the ice divide. The glacier
140 thus remains locked into a state that is similar to the fully retreated state after ice-shelf ungrounding (Fig. 3c).

Out of the nine sets of hysteresis experiments, three yield reversible GL evolution (marked "R" in Fig. 4), four a hysteretic behavior ("H") and two show a lock-in effect ("L"). The type of response depends on the bed-topographic configuration, i.e., on the combination of the size of the bed depression and the location of the topographic high (Fig. 1b). As can be seen from
145 Fig. 4, a deeper bed depression and a topographic high that has a larger distance from the ice divide favor hysteretic and lock-in behavior.

In each series of experiments the retreating GL eventually passes the deepest point of the bed depression, finding a final stable position on the prograde bed section upstream of the bed depression (Figs. 1b and 2). A flat bed depression and/or a topographic-high location less distant from the ice divide lead to more gradual steps of GL retreat between two subsequent
150 experiments (on the order of 10 km; see panel a in Figs. 3 and S1-3). In contrast, a deep bed depression and a more distant



topographic-high location foster an abrupt change in GL position ($\gtrsim 200$ km) once the topographic-high depth crosses a certain threshold, resulting in a steep hysteresis curve (red curves in panels b and c of Figs. 3 and S1-S4). Thus, in these experiments the simulated glacier tips from a relatively large, advanced state (GL on coastal sill) into a small, collapsed state (GL on inland sill, Fig. 2). During this MISI-type retreat the ice shelf remains pinned on the topographic high.

155 Reversal of the perturbation leads to the re-grounding of the ice shelf on the topographic high and, in the course of the step-wise elevation of the topographic high, the GL re-advances into the bed depression. A deeper bed depression and a more distant topographic high hamper the GL in passing the depression (Figs. 3 and S1-S3). Consequently, larger D_{BD} and/or x_{TH} increase the gap between the two curves in the hysteresis diagram (denoted by ΔD_{TH} in Figs. 3b and 4). This gap measures the amount of additional change in the forcing, required to tip back the glacier from its collapsed to its advanced state on
160 the path of regrowth (blue curves in Figs. 3b, S2b,c and S3b) compared to the path of retreat. In other words, ΔD_{TH} is the additional increase of the topographic-high elevation required to induce GL re-advance from the bed depression onto the coastal sill, compared to the reversible case (corresponding to $\Delta D_{TH} = 0$). If the depth of the bed depression and the distance of the topographic high are sufficiently large, the GL does not pass the depression in downstream direction in the course of the elevation increase of the topographic high and the glacier remains in a collapsed state (Figs. 2c and f).

165 3.2 Laterally unconfined simulations

For more insight into why the glacier response behavior is affected by the depth of the bed depression and the distance of the pinning point, we conduct a small set of additional experiments to examine the glacier's flux balance under flowline conditions. For this purpose we have removed the lateral confinement of the prescribed bed topography by doubling the bed-trough width and cutting off the computational domain at $y = \pm 80$ km (compare Figs. S6a to S7a), referring to these modified simulations
170 as laterally unconfined in the following. In the flow band around the centerline of the computational domain the bed profiles of the laterally unconfined setup and the laterally confined setup are the same. Since in the laterally unconfined case the simulated ice stream is not restrained laterally, its flow is generally in x direction and the y component of the velocity field is non-zero only in the vicinity of the ice-shelf pinning point (compare Figs. S6b to S7b). We make use of these flowline conditions that prevail far enough upstream of the pinning point in a flux balance analysis that is presented in Sect. 3.2.1.

175 Note that in the laterally unconfined simulations the ice-shelf pinning on the topographic high is the only source of buttressing compared to the laterally confined experiments in which the central pinning-point buttressing is complemented by a backforce generated at the lateral shear margins of the ice shelf. The reduced backstress on the upstream grounded ice implies a larger ice discharge across the GL (outflux) with major implications for the steady states and the glacier response in the laterally unconfined case: 1) Without any modifications, the model initialization would result in a much smaller outlet compared to the laterally confined case. To compensate for this effect we prescribe a substantially higher surface accumulation rate
180 ($a = 1 \text{ ma}^{-1}$ instead of 0.15 ma^{-1}) in the laterally unconfined setup, obtaining an initial steady-state glacier profile that is qualitatively comparable to the laterally confined case (compare Figs. 2 to S5). For consistency, the other model parameters are left unchanged. 2) The step-wise reduction in pinning-point buttressing eventually leads to the complete disintegration of the



grounded ice sheet even before the ice shelf ungrounds from the topographic high. 3) The re-advance of the GL in response to
 185 raising the topographic high is strongly limited compared to the laterally confined case. In fact, in the absence of confinement-
 induced buttressing, pinning-point buttressing is insufficient to cause glacier re-advance toward its original state even for the
 case of a flat bed depression and a much higher topographic-high elevation than the original value (Figs. S4 and S5).

3.2.1 Flowline flux balance analysis

In the laterally unconfined case, the velocity of the ice-sheet-shelf system is zero in the y -dimension for the region upstream of
 190 $x = 400$ km (see straight velocity contours in Fig. S7b), where it thus can be treated as a flowline ice stream in x direction. In
 the collapsed state, i.e., when the grounded part of the glacier has retreated onto the inland sill and is thus located far upstream
 of the pinning point, the GL is straight and parallel to the velocity contours. For such a buttressed glacier in flowline, the
 steady-state ice discharge across the GL, i.e., the outflux $Q_o(x_{GL})$, can be calculated analytically according to the boundary
 layer theory by Schoof (2007, Eq. 29),

$$195 \quad Q_o(x_{GL}) = -c \Theta(x_{GL})^{\frac{n}{m+1}} B(x_{GL})^{\frac{m+n+3}{m+1}}, \quad (4)$$

as a function of the bed elevation, $B(x_{GL})$, and the buttressing ratio $\Theta(x_{GL})$ at the GL position, x_{GL} , respectively (Schoof,
 2007; Gudmundsson et al., 2023). The parameter n denotes the exponent in Glen's flow law (Glen, 1955) and m is the exponent
 in the Weertman friction law (Cornford et al., 2020, Eq. 3). The factor c is constant in space and time,

$$c = \left(\frac{A(\rho_i g)^{n+1} (1 - \rho_i / \rho_o)^n}{4^n C} \right)^{\frac{1}{m+1}}, \quad (5)$$

200 in which A is the ice softness, C is the basal-friction coefficient, g denotes the gravitational acceleration and ρ_i and ρ_o , are the
 ice and ocean densities, respectively (values for all parameters given in Table 1). Note that, as we are considering marine outlet
 glaciers, $B(x_{GL})$ is always negative and since $c > 0$ the outflux $Q_o(x_{GL})$ is positive.

For the parameter values used in our experiments, Eq. (4) reads

$$Q_o(x_{GL}) = -c \Theta(x_{GL})^{\frac{9}{4}} B(x_{GL})^{\frac{19}{4}}. \quad (6)$$

205 The buttressing ratio, $\Theta(x_{GL})$, relates the ice-internal stresses at the GL to the stresses exerted at the calving front due to
 ocean pressure. If $\Theta(x_{GL}) < 1$, the stresses at the GL are smaller compared to the ocean pressure and the ice shelf provides
 buttressing, reducing the GL flux. If $\Theta(x_{GL}) > 1$, the opposite is the case, i.e., traction at the GL is larger than the ocean
 pressure, which means that the ice shelf is "pulling" which increases the ice discharge across the GL (Gudmundsson, 2013).
 In case of $\Theta(x_{GL}) = 1$, the presence of the ice shelf has no effect on the upstream stresses, i.e., the stresses at the GL are
 210 equal to the ocean pressure at the calving front. For instance, such conditions prevail in the the absence of pinning points
 for an unconfined ice shelf in the flowline case (only one horizontal dimension), such that the ice shelf does not provide any
 buttressing nor "pulls" the flow at the GL. In this case, the GL flux depends solely on the bed topography and thus Eq. (6)
 reduces to

$$Q_o(x_{GL}) = -c B(x_{GL})^{\frac{19}{4}}. \quad (7)$$



215 This function is visualized by the grey curves in Figs. 5e and f for the centerline profile of the bed depression, demonstrating how the bed profile is mirrored by the GL flux in a highly non-linear way. In case of a deep bed depression the peak of the flux curve is much larger than in the shallow case (flux larger by about 400 % for a 33 % deeper depression). Note that this curve gives the steady-state ice discharge for any potential GL position along the bed profile. For an outlet glacier in equilibrium, this outflux Q_o has to be balanced by an influx Q_i which in flowline is given by the integral of the surface accumulation rate a
220 between the ice divide ($x = 0$) and the GL position, i.e.,

$$Q_i = a x_{GL}. \quad (8)$$

The slope of this linear function in x_{GL} is determined by the surface accumulation rate (black curves in Figs. 5e and f). For the parameters and bed topographies prescribed in our experiments, the curves of in- and outflux do not intersect in the absence of buttressing, and thus a steady-state outlet glacier cannot exist in this configuration according to the analytical calculations.
225 This is in agreement with our laterally unconfined simulations in which the glacier retreats all the way to the ice divide and thus vanishes in the course of the step-wise topographic-high lowering (and thus buttressing reduction) for a pinning-point depth of $D_{TH} = 300$ m even before it's ice shelf ungrounds from the topographic high (Fig. S5).

Reverting the perturbation sequence at this stage, i.e., reducing the topographic-high depth to $D_{TH} = 280$ m, leads to buttressing-induced ice shelf thickening that is sufficient to cause the re-grounding of the ice shelf on the inland sill such
230 that a small glacier re-emerges ($x_{GL} > 0$; Fig. S4). Now the curves of in- and outflux have an intersection (Figs. 5e and f), predicting a stable GL position since Q_o increases faster than Q_i at the GL (Schoof, 2012). In the following, we focus on the subsequent glacier re-advance in response to the step-wise increase in the topographic-high elevation. The backstress exerted by the ice-shelf pinning point on the upstream ice is associated with values of $\Theta < 1$. This can be seen from the steady-state flowline profiles of Θ which we infer from the simulations, based on the traction normal to the GL along the centerline of the
235 setup (Figs. 5c and d). Note that in a strict sense, Θ may only be evaluated at the GL position to calculate the GL flux Q_o corresponding to the steady state. Thus, the resulting curves from calculating Q_o for the profile of Θ show the theoretical GL flux under the assumption that the Θ profile would not change for a change in the GL position. That is, the gap between the Q_o profiles and Q_i at a location x downstream of the GL can be interpreted as the additional amount of flux reduction that would be required to advance the GL to this location but is not provided under the buttressing conditions of the current steady state.

240 In the vicinity of the GL, the diagnosed Θ values range roughly between 0.4 and 0.65 with the lower values corresponding to higher topographic-high elevations, i.e., stronger pinning-point buttressing. As can be seen from the colored curves in Figs. 5e and f, the pinning-point buttressing leads to a flattening (vertical compression) of the GL flux profile compared to the unbuttressed case (compare to grey curves associated with $\Theta = 1$). In fact, this reduction in GL flux allows for stable solutions of the GL position as can be seen from the intersects between in- and outflux curves and the simulated glacier profiles. With
245 increasing pinning-point buttressing, i.e., increasing topographic-high elevation, the flattening of the curves becomes more pronounced (Figs. 5e and f). In case of a shallow depression, the gap between the curves of in- and outflux becomes very small for the entire overdeepening (Fig. 5e). These conditions ease the advance of the GL within the region of the bed depression. The



situation is different in the deep-depression case, in which, despite the pinning-point induced reduction in outflux, a substantial gap between the curves of in- and outflux remains along the central part of the overdeepening (outflux about one order of magnitude larger than influx at the deepest point of the bed depression; see Fig. 5f). With similar buttressing values compared to the flat-depression case, the compensation of the much larger GL flux due to the deeper bed depression remains much more limited, resulting in diminished GL advance.

In the laterally unconfined setup, pinning-point buttressing turns out to be too weak to induce glacier re-advance toward its original state and the glacier remains in a collapsed state even for the case of a flat bed depression (Fig. S4). Consequently, our analysis can not explicitly prove that a flatter bed depression can revert glacier collapse as found in the laterally confined simulations. However, our results from applying the flowline flux balance analysis provide a theory-based reasoning of why a shallower bed depression in combination with ice-shelf buttressing does facilitate glacier re-advance (and potential full recovery) after MISI-type retreat.

4 Discussion

Our simulations demonstrate how an idealized MISI-prone outlet glacier that is stabilized on retrograde bed by pinning-point induced buttressing can undergo rapid and irreversible retreat in response to a relatively small buttressing reduction. The prescribed bed topography plays a key role in determining (ir-)reversibility of glacier retreat and re-advance. Our topographic setup (Fig. 1) is based on previous studies (Gudmundsson et al., 2012; Cornford et al., 2020) that simulated a stable GL position on retrograde bed in the absence of pinning-point buttressing. In those experiments buttressing was provided exclusively due to the relatively narrow to moderate bed trough confining the streaming trunk of the glacier laterally (prescribed confinement widths of roughly 50 to 100 km). Here we use a much wider confinement width of 160 km which is similar to the observed width of Thwaites Glacier's fast flowing trunk at the GL (e.g., Davison et al., 2023, Fig. 1a). In the absence of a pinning point, such a confinement would be too wide to prevent glacier collapse during model initialization, as we have shown in earlier simulations (Feldmann and Levermann, 2023). This is consistent with results from Goldberg et al. (2009) who also found that ice-shelf grounding on a central topographic high can prevent MISI-type retreat and concluded that the presence of such a pinning point can have a similar effect as halving the ice-shelf width (and thus increasing the buttressing effect based on parameterized lateral drag at the ice-shelf margins). In the present study, GL stabilization on the retrograde slope takes place for topographic-high elevations between -380 and -40 m (Figs. 3, S2 and S3). According to our results, a steeper retrograde slope and a larger distance of the pinning point from the ice divide require higher topographic-high elevations, associated with a stronger buttressing effect of the pinning point. Antarctic-wide mean elevations of ice rises and ice rumples, calculated from present-day observations, range from about -200 to -300 m (Matsuoka et al., 2015).

In our simulations, the GL destabilizes once the topographic-high elevation is lowered beyond a critical threshold but only if the glacier rests on a sufficiently deep bed depression (Figs. 3, and S1-S3). This is in agreement with analytical results from Schoof (2012) who found that the GL of an idealized, unbuttressed marine ice sheet can have stable steady states on



280 sufficiently shallow retrograde bed slope for the flowline case (one horizontal dimension). In our laterally confined simulations,
that comprise both horizontal dimensions, ice-shelf buttressing emerges as a combination of 1) horizontal shearing within the
ice at the lateral, topographically confined ice-stream margins (confinement-induced buttressing) and 2) basal drag where the
ice shelf is pinned on the topographic high (pinning-point induced buttressing). In the laterally unconfined simulations the
pinning point is the only source of buttressing. The comparison to the laterally confined simulations reveals that the additional
285 buttressing effect of a laterally confined ice shelf facilitates glacier re-advance substantially since in the laterally unconfined
experiments the glacier remains locked in its collapsed state even for the flattest bed depression and a substantially higher
surface accumulation rate. The 500-m deep and 160-km wide topographic confinement, prescribed in the laterally confined
simulations, strongly confines the fast glacier (ice-stream) flow throughout the entire length of the computational domain. In
contrast to that, the observed fast flowing trunk of Thwaites Glacier is much less confined by the subglacial bed topography and
290 it's width increases into the interior, doubling to about 300 km over the first 200 km upstream of the present-day GL (Davison
et al., 2023).

A characteristic outcome of our experiments is that outlets which rest on a deeper bed depression and which are less but-
tressed, generally show a greater susceptibility to abrupt and irreversible (MISI-type) retreat (Figs. 3, 4 and S1-S3). Applying
our results to the real world in a qualitative sense, we thus expect that wider, laterally weakly confined outlet glaciers like
295 Thwaites Glacier would be more susceptible to abrupt retreat and more likely exhibit hysteretic/lock-in behavior than narrower
outlets with a strong topographic confinement like Pine Island Glacier (MacGregor et al., 2013; Rignot et al., 2014; Morlighem
et al., 2020; Schwans et al., 2023). The many differences between our idealized simulations and nature limit particularly
the quantitative applicability of our results to the real world. In the following we discuss several simplifying aspects of our
simulations and how they affect our results.

300 The perturbations applied in our simulations are of synthetic character and would not be observed in nature. However,
prescribing changes of the topographic-high elevation serves as a direct and minimal-invasive control of pinning-point induced
buttressing. In real world, changes in pinning-point buttressing would result from ice-shelf thickness changes (due to sub-
ice-shelf melting/refreezing; Reese et al., 2018; Gudmundsson et al., 2019), ice-shelf weakening/fracturing in the vicinity of
the pinning point (Benn et al., 2022; Sun and Gudmundsson, 2023; Surawy-Stepney et al., 2023), iceberg calving (Arndt
305 et al., 2018) or glacial isostatic adjustment (GIA; Matsuoka et al., 2015). We chose the magnitude of the perturbation steps
as compromise between the graduality of pinning-point buttressing change and the number of numerical simulations, i.e.,
the computational cost. Smaller perturbation steps would in particular allow for a more accurate quantification of the critical
thresholds of abrupt GL retreat and re-advance, but leave the conclusions of our study unchanged.

Our simulations neglect basal ice-shelf melting which is an important driver of Antarctic ice-sheet dynamics, shaping the
310 geometry of ice shelves, often reducing their buttressing effect and thus increasing the discharge of the outlet glaciers around
Antarctica (Dutrieux et al., 2013; Reese et al., 2018; Gudmundsson et al., 2019). The inclusion of basal melting in our simula-
tions would lead to an overall thinner ice shelf, facilitating ice-shelf unpinning (GL retreat) and hampering re-grounding (GL



advance). This might expand the regimes of hysteretic and lock-in behavior at the expense of the reversibility regime in our parameter space. In fact, due to the incremental thickening of the ice shelf with increasing topographic-high elevation, even
315 in the simulated lock-in cases the glacier is expected to eventually re-advance to its original state due to thickening-induced ice-shelf grounding on the upstream side of the coastal sill (note the proximity of the ice-shelf draft to the sill in Figs. 2c and f). Since the ice-shelf thickness is approximately uniform across the entire bed trough (except for the vicinity of the topographic high), the grounding of the ice shelf upstream of the coastal sill would cover the entire bed-trough width and thus lead to a closing of the ice-shelf cavity. That is, a water volume on the order of 1000 km^3 (10^{15} L) would be trapped within the bed
320 depression, confined by the ice-shelf draft at the top, the overdeepened bed at the bottom and the lateral walls of the bed trough.

Prescribing a fixed bed topography in each simulation, we neglect possible GIA effects (Matsuoka et al., 2015; Barletta et al., 2018). A rebound of the bed induced by glacier retreat would reduce the depth of the bed depression and thus facilitate glacier re-advance. Including GIA in our simulations could thus counteract the lock-in effect observed for the deepest bed depression used in our simulations and shift the lock-in regime into regions of greater bed-depression depth. Note that the bed depressions
325 (and thus the bed slopes) chosen here are rather less pronounced compared to observations in the Amundsen Sea Embayment. For instance, the bed along a central transect through Thwaites Glacier drops by about -750 m over the first 250 km upstream of the GL, resulting in an average bed slope of $s \approx -3 \cdot 10^{-3}$ (Morlighem et al., 2020; Sergienko and Wingham, 2022). In our simulations the steepest part of the retrograde slope has values of $s_{D_{\text{BD}}=675} \approx -3.75 \cdot 10^{-4}$, $s_{D_{\text{BD}}=750} \approx -7.5 \cdot 10^{-4}$, $s_{D_{\text{BD}}=900} \approx -1.5 \cdot 10^{-3}$, for the three different depths of the overdeepening, respectively.

330 Variations in basal friction (between ice and bed) are not investigated in our study. A comparison between Ross Ice Shelf's various pinning points concluded that the magnitude of their effective resistance to the ice flow does not only depend on the area and elevation of the pinning point but also on the nature of the subglacial material on which the ice shelf is grounded (Still et al., 2019). Idealized simulations showed that a higher degree of friction at the ice-bed interface favors the emergence of pinning points of larger horizontal extent which provide more buttressing to the upstream flow (Henry et al., 2022). Consequently, we
335 expect that a stronger basal resistance would favor reversibility of retreat and advance.

5 Conclusions

Our idealized simulations highlight that the stability and (ir-)reversible migration of MISI-prone outlet glaciers can be strongly affected by the interplay of 1) variations in pinning-point buttressing and 2) the depth of their subglacial bed depression. Abrupt, unstable GL retreat (MISI) occurs for sufficiently steep retrograde slopes once a critical perturbation threshold (elevation of
340 the topographic high that controls the buttressing strength of the pinning point) is crossed (Figs. 3 and S1-S3). This retreat is irreversible, meaning that glacier re-advance under reversal of the perturbation is either of hysteretic nature or so marginal that the glacier remains locked in a collapsed state (Figs. 2 and 4). Conversely, in case of a comparatively flat retrograde slope, glacier retreat and re-advance follow the perturbation sequence gradually and are reversible. However, in the absence of the



strong lateral topographic confinement (substantially diminished overall ice-shelf buttressing), the glacier does not recover
345 from its collapsed state even for a shallow bed depression (Figs. 5, S4 and S5).

While the application of our results to the real world is limited in a quantitative sense due to the idealized nature of our
simulations, our findings qualitatively suggest that outlets that rest on a deep bed depression and are weakly buttressed, such
as Thwaites Glacier, are more susceptible to abrupt and irreversible (MISI-type) retreat than stronger buttressed glaciers on
more moderate retrograde slope, such as Pine Island Glacier. In particular, our results highlight that the bed-topographic
350 configuration of Thwaites Glacier with its very wide marine drainage basin that drops into one of the deepest regions of the
Antarctic continent does not only provide favorable conditions for unstable retreat but also would strongly hamper possible
glacier re-advance after a potential collapse.

Code and data availability. The model code used in this study is based on PISM stable version 1.0 and can be obtained from
<https://doi.org/10.5281/zenodo.6531439> (Feldmann, 2022)

355 .

Author contributions. JF designed the study and performed the numerical simulations. JF prepared the figures and the manuscript with
contributions from AL and RW.

Competing interests. The contact author has declared that none of the authors has any competing interests.

Acknowledgements. This work was supported by the Deutsche Forschungsgemeinschaft (DFG) in the framework of the priority programme
360 "Antarctic Research with comparative investigations in Arctic ice areas" SPP 1158 through grant WI 4556/6-1. JF and RW are grateful
for support by the European Union's Horizon 2020 research and innovation programme under Grant Agreement No. 820575 (TiPACCs).
RW further acknowledges support by the European Union's Horizon 2020 research and innovation programme under Grant Agreement
No. 869304 (PROTECT). Development of PISM is supported by NASA grants 20-CRYO2020-0052 and 80NSSC22K0274 and NSF grant
OAC-2118285. The authors gratefully acknowledge the European Regional Development Fund (ERDF), the German Federal Ministry of
365 Education and Research and the Land Brandenburg for supporting this project by providing resources on the high performance computer
system at the Potsdam Institute for Climate Impact Research.



References

- Alley, K. E., Wild, C. T., Luckman, A., Scambos, T. A., Truffer, M., Pettit, E. C., Muto, A., Wallin, B., Klinger, M., Sutterley, T., Child, S. F., Hulén, C., Lenaerts, J. T. M., Maclennan, M., Keenan, E., and Dunmire, D.: Two decades of dynamic change and progressive destabilization on the Thwaites Eastern Ice Shelf, *The Cryosphere*, 15, 5187–5203, <https://doi.org/10.5194/tc-15-5187-2021>, publisher: Copernicus GmbH, 2021.
- Arndt, J. E., Larter, R. D., Friedl, P., Gohl, K., Höppner, K., and the Science Team of Expedition PS104: Bathymetric controls on calving processes at Pine Island Glacier, *The Cryosphere*, 12, 2039–2050, <https://doi.org/10.5194/tc-12-2039-2018>, publisher: Copernicus GmbH, 2018.
- Asay-Davis, X. S., Cornford, S. L., Durand, G., Galton-Fenzi, B. K., Gladstone, R. M., Gudmundsson, G. H., Hattermann, T., Holland, D. M., Holland, D., Holland, P. R., Martin, D. F., Mathiot, P., Pattyn, F., and Seroussi, H.: Experimental design for three interrelated marine ice sheet and ocean model intercomparison projects: MISMIP v. 3 (MISMIP +), ISOMIP v. 2 (ISOMIP +) and MISOMIP v. 1 (MISOMIP1), *Geoscientific Model Development*, 9, 2471–2497, <https://doi.org/10.5194/gmd-9-2471-2016>, 2016.
- Bamber, J. L., Riva, R. E. M., Vermeersen, B. L. A., and LeBrocq, A. M.: Reassessment of the Potential Sea-Level Rise from a Collapse of the West Antarctic Ice Sheet, *Science*, 324, 901–903, <https://doi.org/10.1126/science.1169335>, 2009.
- Barletta, V. R., Bevis, M., Smith, B. E., Wilson, T., Brown, A., Bordoni, A., Willis, M., Khan, S. A., Rovira-Navarro, M., Dalziel, I., Smalley, R., Kendrick, E., Konfal, S., Caccamise, D. J., Aster, R. C., Nyblade, A., and Wiens, D. A.: Observed rapid bedrock uplift in Amundsen Sea Embayment promotes ice-sheet stability, *Science*, 360, 1335–1339, <https://doi.org/10.1126/science.aao1447>, publisher: American Association for the Advancement of Science, 2018.
- Benn, D. I., Luckman, A., Åström, J. A., Crawford, A. J., Cornford, S. L., Bevan, S. L., Zwinger, T., Gladstone, R., Alley, K., Pettit, E., and Bassis, J.: Rapid fragmentation of Thwaites Eastern Ice Shelf, *The Cryosphere*, 16, 2545–2564, <https://doi.org/10.5194/tc-16-2545-2022>, publisher: Copernicus GmbH, 2022.
- Berger, S., Favier, L., Drews, R., Derwael, J.-J., and Pattyn, F.: The control of an uncharted pinning point on the flow of an Antarctic ice shelf, *Journal of Glaciology*, 62, 37–45, <https://doi.org/10.1017/jog.2016.7>, 2016.
- Bett, D. T., Bradley, A. T., Williams, C. R., Holland, P. R., Arthern, R. J., and Goldberg, D. N.: Coupled ice/ocean interactions during the future retreat of West Antarctic ice streams, *The Cryosphere Discussions*, pp. 1–28, <https://doi.org/10.5194/tc-2023-77>, publisher: Copernicus GmbH, 2023.
- Borstad, C. P., Rignot, E., Mouginot, J., and Schodlok, M. P.: Creep deformation and buttressing capacity of damaged ice shelves: theory and application to Larsen C ice shelf, *The Cryosphere*, 7, 1931–1947, <https://doi.org/10.5194/tc-7-1931-2013>, 2013.
- Bronckx, J., Gagliardini, O., Gillet-Chaulet, F., and Durand, G.: Sensitivity of grounding line dynamics to the choice of the friction law, *Journal of Glaciology*, 63, 854–866, <https://doi.org/10.1017/jog.2017.51>, 2017.
- Bueler, E. and Brown, J.: Shallow shelf approximation as a “sliding law” in a thermomechanically coupled ice sheet model, *Journal of Geophysical Research*, 114, F03 008, <https://doi.org/10.1029/2008JF001179>, 2009.
- Christie, F. D. W., Steig, E. J., Gourmelen, N., Tett, S. F. B., and Bingham, R. G.: Inter-decadal climate variability induces differential ice response along Pacific-facing West Antarctica, *Nature Communications*, 14, 93, <https://doi.org/10.1038/s41467-022-35471-3>, number: 1 Publisher: Nature Publishing Group, 2023.
- Cornford, S. L., Seroussi, H., Asay-Davis, X. S., Gudmundsson, G. H., Arthern, R., Borstad, C., Christmann, J., Dias dos Santos, T., Feldmann, J., Goldberg, D., Hoffman, M. J., Humbert, A., Kleiner, T., Leguy, G., Lipscomb, W. H., Merino, N., Durand, G., Morlighem, M.,



- Pollard, D., Rückamp, M., Williams, C. R., and Yu, H.: Results of the third Marine Ice Sheet Model Intercomparison Project (MISMIP+),
405 The Cryosphere, 14, 2283–2301, <https://doi.org/https://doi.org/10.5194/tc-14-2283-2020>, 2020.
- Davison, B. J., Hogg, A. E., Rigby, R., Veldhuijsen, S., van Wessem, J. M., van den Broeke, M. R., Holland, P. R., Selley, H. L., and Dutrioux,
P.: Sea level rise from West Antarctic mass loss significantly modified by large snowfall anomalies, Nature Communications, 14, 1479,
<https://doi.org/10.1038/s41467-023-36990-3>, number: 1 Publisher: Nature Publishing Group, 2023.
- De Rydt, J., Reese, R., Paolo, F. S., and Gudmundsson, G. H.: Drivers of Pine Island Glacier speed-up between 1996 and 2016, The
410 Cryosphere, 15, 113–132, <https://doi.org/10.5194/tc-15-113-2021>, publisher: Copernicus GmbH, 2021.
- Dupont, T. K. and Alley, R. B.: Assessment of the importance of ice-shelf buttressing to ice-sheet flow, Geophysical Research Letters, 32,
L04 503, <https://doi.org/10.1029/2004GL022024>, 2005.
- Dutrioux, P., Vaughan, D. G., Corr, H. F. J., Jenkins, A., Holland, P. R., Joughin, I., and Fleming, A. H.: Pine Island glacier ice shelf melt
distributed at kilometre scales, The Cryosphere, 7, 1543–1555, <https://doi.org/10.5194/tc-7-1543-2013>, 2013.
- 415 Favier, L. and Pattyn, F.: Antarctic ice rise formation, evolution, and stability: ICE-RISES FORMATION, Geophysical Research Letters, 42,
4456–4463, <https://doi.org/10.1002/2015GL064195>, 2015.
- Favier, L., Gagliardini, O., Durand, G., and Zwinger, T.: A three-dimensional full Stokes model of the grounding line dynamics: effect of a
pinning point beneath the ice shelf, The Cryosphere, 6, 101–112, <https://doi.org/10.5194/tc-6-101-2012>, 2012.
- Favier, L., Pattyn, F., Berger, S., and Drews, R.: Dynamic influence of pinning points on marine ice-sheet stability: a numerical study in
420 Dronning Maud Land, East Antarctica, The Cryosphere, 10, 2623–2635, <https://doi.org/10.5194/tc-10-2623-2016>, publisher: Copernicus
GmbH, 2016.
- Feldmann, J.: PISM model code as used in this study (stable v1.0-1843-g803f50dac), <https://doi.org/10.5281/zenodo.6531439>, 2022.
- Feldmann, J. and Levermann, A.: Collapse of the West Antarctic Ice Sheet after local destabilization of the Amundsen Basin, Proceedings of
the National Academy of Sciences, 112, 14 191–14 196, <https://doi.org/10.1073/pnas.1512482112>, 2015.
- 425 Feldmann, J. and Levermann, A.: Timescales of outlet-glacier flow with negligible basal friction: theory, observations and modeling, The
Cryosphere, 17, 327–348, <https://doi.org/10.5194/tc-17-327-2023>, publisher: Copernicus GmbH, 2023.
- Feldmann, J., Albrecht, T., Khroulev, C., Pattyn, F., and Levermann, A.: Resolution-dependent performance of grounding line motion in
a shallow model compared with a full-Stokes model according to the MISMIP3d intercomparison, Journal of Glaciology, 60, 353–360,
<https://doi.org/10.3189/2014JoG13J093>, 2014.
- 430 Fürst, J. J., Durand, G., Gillet-Chaulet, F., Tavard, L., Rankl, M., Braun, M., and Gagliardini, O.: The safety band of Antarctic ice shelves,
Nature Climate Change, 6, 479–482, <https://doi.org/10.1038/nclimate2912>, 2016.
- Gagliardini, O., Durand, G., Zwinger, T., Hindmarsh, R. C. A., and Le Meur, E.: Coupling of ice-shelf melting and buttressing is
a key process in ice-sheets dynamics: ICE-SHELF MELTING AND BUTTRESSING, Geophysical Research Letters, 37, n/a–n/a,
<https://doi.org/10.1029/2010GL043334>, 2010.
- 435 Glen, J. W.: The creep of polycrystalline ice, Proceedings of the Royal Society of London. Series A. Mathematical and Physical Sciences,
228, 519–538, <https://doi.org/10.1098/rspa.1955.0066>, publisher: Royal Society, 1955.
- Goldberg, D., Holland, D. M., and Schoof, C.: Grounding line movement and ice shelf buttressing in marine ice sheets, Journal of Geophysical
Research, 114, F04 026, <https://doi.org/10.1029/2008JF001227>, 2009.
- Greve, R. and Blatter, H.: Dynamics of Ice Sheets and Glaciers, Advances in Geophysical and Environmental Mechanics and Mathematics,
440 Springer Berlin Heidelberg, Berlin, Heidelberg, <https://doi.org/10.1007/978-3-642-03415-2>, 2009.



- Gudmundsson, G. H.: Ice-shelf buttressing and the stability of marine ice sheets, *The Cryosphere*, 7, 647–655, <https://doi.org/10.5194/tc-7-647-2013>, 2013.
- Gudmundsson, G. H., Krug, J., Durand, G., Favier, L., and Gagliardini, O.: The stability of grounding lines on retrograde slopes, *The Cryosphere*, 6, 1497–1505, <https://doi.org/10.5194/tc-6-1497-2012>, 2012.
- 445 Gudmundsson, G. H., Rydt, J. D., and Nagler, T.: Five decades of strong temporal variability in the flow of Brunt Ice Shelf, Antarctica, *Journal of Glaciology*, 63, 164–175, <https://doi.org/10.1017/jog.2016.132>, publisher: Cambridge University Press, 2017.
- Gudmundsson, G. H., Paolo, F. S., Adusumilli, S., and Fricker, H. A.: Instantaneous Antarctic ice sheet mass loss driven by thinning ice shelves, *Geophysical Research Letters*, 46, 13 903–13 909, <https://doi.org/10.1029/2019GL085027>, <https://onlinelibrary.wiley.com/doi/pdf/10.1029/2019GL085027>, 2019.
- 450 Gudmundsson, G. H., Barnes, J. M., Goldberg, D. N., and Morlighem, M.: Limited Impact of Thwaites Ice Shelf on Future Ice Loss From Antarctica, *Geophysical Research Letters*, 50, e2023GL102 880, <https://doi.org/10.1029/2023GL102880>, <https://onlinelibrary.wiley.com/doi/pdf/10.1029/2023GL102880>, 2023.
- Henry, A. C. J., Drews, R., Schannwell, C., and Višnjević, V.: Hysteretic evolution of ice rises and ice rumples in response to variations in sea level, *The Cryosphere*, 16, 3889–3905, <https://doi.org/10.5194/tc-16-3889-2022>, publisher: Copernicus GmbH, 2022.
- 455 Hutter, K.: *Theoretical Glaciology: Material Science of Ice and the Mechanics of Glaciers and Ice Sheets (Mathematical Approaches to Geophysics)*, Reidel Publishing Company/Terra Scientific Publishing Company, 1983.
- Joughin, I., Shapero, D., Smith, B., Dutrioux, P., and Barham, M.: Ice-shelf retreat drives recent Pine Island Glacier speedup, *Science Advances*, 7, eabg3080, <https://doi.org/10.1126/sciadv.abg3080>, publisher: American Association for the Advancement of Science Section: Research Article, 2021.
- 460 Konrad, H., Shepherd, A., Gilbert, L., Hogg, A. E., McMillan, M., Muir, A., and Slater, T.: Net retreat of Antarctic glacier grounding lines, *Nature Geoscience*, 11, 258–262, <https://doi.org/10.1038/s41561-018-0082-z>, 2018.
- Macayeal, D. R., Bindschadler, R. A., Shabtaie, S., Stephenson, S., and Bentley, C. R.: Force, Mass, and Energy Budgets of the Crary Ice Rise Complex, Antarctica, *Journal of Glaciology*, 33, 218–230, <https://doi.org/10.3189/S0022143000008728>, publisher: Cambridge University Press, 1987.
- 465 MacGregor, J. A., Catania, G. A., Markowski, M. S., and Andrews, A. G.: Widespread rifting and retreat of ice-shelf margins in the eastern Amundsen Sea Embayment between 1972 and 2011, *Journal of Glaciology*, 58, 458–466, <https://doi.org/10.3189/2012JoG11J262>, publisher: Cambridge University Press, 2012.
- MacGregor, J. A., Catania, G. A., Conway, H., Schroeder, D. M., Joughin, I., Young, D. A., Kempf, S. D., and Blankenship, D. D.: Weak bed control of the eastern shear margin of Thwaites Glacier, West Antarctica, *Journal of Glaciology*, 59, 900–912, <https://doi.org/10.3189/2013JoG13J050>, publisher: Cambridge University Press, 2013.
- 470 Matsuoka, K., Hindmarsh, R. C. A., Moholdt, G., Bentley, M. J., Pritchard, H. D., Brown, J., Conway, H., Drews, R., Durand, G., Goldberg, D., Hattermann, T., Kingslake, J., Lenaerts, J. T. M., Martín, C., Mulvaney, R., Nicholls, K. W., Pattyn, F., Ross, N., Scambos, T., and Whitehouse, P. L.: Antarctic ice rises and rumples: Their properties and significance for ice-sheet dynamics and evolution, *Earth-Science Reviews*, 150, 724–745, <https://doi.org/10.1016/j.earscirev.2015.09.004>, 2015.
- 475 Mercer, J. H.: West Antarctic ice sheet and CO₂ greenhouse effect: a threat of disaster, *Nature*, 271, 321–325, <https://doi.org/10.1038/271321a0>, 1978.
- Milillo, P., Rignot, E., Rizzoli, P., Scheuchl, B., Mouginit, J., Bueso-Bello, J., and Prats-Iraola, P.: Heterogeneous retreat and ice melt of Thwaites Glacier, West Antarctica, *Science Advances*, 5, eaau3433, <https://doi.org/10.1126/sciadv.aau3433>, 2019.



- Milillo, P., Rignot, E., Rizzoli, P., Scheuchl, B., Mouginot, J., Bueso-Bello, J. L., Prats-Iraola, P., and Dini, L.: Rapid glacier retreat rates observed in West Antarctica, *Nature Geoscience*, 15, 48–53, <https://doi.org/10.1038/s41561-021-00877-z>, number: 1 Publisher: Nature Publishing Group, 2022.
- Morland, L. W.: Unconfined Ice-Shelf Flow, in: *Dynamics of the West Antarctic Ice Sheet*, edited by Van der Veen, C. J. and Oerlemans, J., *Glaciology and Quaternary Geology*, pp. 99–116, Springer Netherlands, https://doi.org/10.1007/978-94-009-3745-1_6, 1987.
- Morlighem, M., Rignot, E., Binder, T., Blankenship, D., Drews, R., Eagles, G., Eisen, O., Ferraccioli, F., Forsberg, R., Fretwell, P., Goel, V., Greenbaum, J. S., Gudmundsson, H., Guo, J., Helm, V., Hofstede, C., Howat, I., Humbert, A., Jokat, W., Karlsson, N. B., Lee, W. S., Matsuoka, K., Millan, R., Mouginot, J., Paden, J., Pattyn, F., Roberts, J., Rosier, S., Ruppel, A., Seroussi, H., Smith, E. C., Steinhage, D., Sun, B., Broeke, M. R. v. d., Ommen, T. D. v., Wessens, M. v., and Young, D. A.: Deep glacial troughs and stabilizing ridges unveiled beneath the margins of the Antarctic ice sheet, *Nature Geoscience*, 13, 132–137, <https://doi.org/10.1038/s41561-019-0510-8>, 2020.
- Paolo, F. S., Fricker, H. A., and Padman, L.: Volume loss from Antarctic ice shelves is accelerating, *Science*, 348, 327–331, <https://doi.org/10.1126/science.aaa0940>, 2015.
- Pattyn, F.: The paradigm shift in Antarctic ice sheet modelling, *Nature Communications*, 9, 2728, <https://doi.org/10.1038/s41467-018-05003-z>, 2018.
- Pattyn, F., Perichon, L., Durand, G., Favier, L., Gagliardini, O., Hindmarsh, R. C., Zwinger, T., Albrecht, T., Cornford, S., Docquier, D., Fürst, J. J., Goldberg, D., Gudmundsson, G. H., Humbert, A., Hütten, M., Huybrechts, P., Jouvét, G., Kleiner, T., Larour, E., Martin, D., Morlighem, M., Payne, A. J., Pollard, D., Rückamp, M., Rybak, O., Seroussi, H., Thoma, M., and Wilkens, N.: Grounding-line migration in plan-view marine ice-sheet models: results of the ice2sea MISMIP3d intercomparison, *Journal of Glaciology*, 59, 410–422, <https://doi.org/10.3189/2013JoG12J129>, 2013.
- Pegler, S. S.: Suppression of marine ice sheet instability, *Journal of Fluid Mechanics*, 857, 648–680, <https://doi.org/10.1017/jfm.2018.742>, 2018.
- Reese, R., Gudmundsson, G. H., Levermann, A., and Winkelmann, R.: The far reach of ice-shelf thinning in Antarctica, *Nature Climate Change*, 8, 53–57, <https://doi.org/10.1038/s41558-017-0020-x>, 2018.
- Reese, R., Levermann, A., Albrecht, T., Seroussi, H., and Winkelmann, R.: The role of history and strength of the oceanic forcing in sea level projections from Antarctica with the Parallel Ice Sheet Model, *The Cryosphere*, 14, 3097–3110, <https://doi.org/10.5194/tc-14-3097-2020>, publisher: Copernicus GmbH, 2020.
- Reese, R., Garbe, J., Hill, E. A., Urruty, B., Naughten, K. A., Gagliardini, O., Durand, G., Gillet-Chaulet, F., Gudmundsson, G. H., Chandler, D., Langebroek, P. M., and Winkelmann, R.: The stability of present-day Antarctic grounding lines – Part 2: Onset of irreversible retreat of Amundsen Sea glaciers under current climate on centennial timescales cannot be excluded, *The Cryosphere*, 17, 3761–3783, <https://doi.org/10.5194/tc-17-3761-2023>, publisher: Copernicus GmbH, 2023.
- Rignot, E., Mouginot, J., Morlighem, M., Seroussi, H., and Scheuchl, B.: Widespread, rapid grounding line retreat of Pine Island, Thwaites, Smith, and Kohler glaciers, West Antarctica, from 1992 to 2011, *Geophysical Research Letters*, 41, 3502–3509, <https://doi.org/10.1002/2014GL060140>, eprint: <https://onlinelibrary.wiley.com/doi/pdf/10.1002/2014GL060140>, 2014.
- Rignot, E., Mouginot, J., Scheuchl, B., and Jeong, S.: Changes in Antarctic Ice Sheet Motion Derived From Satellite Radar Interferometry Between 1995 and 2022, *Geophysical Research Letters*, 49, e2022GL100141, <https://doi.org/10.1029/2022GL100141>, eprint: <https://onlinelibrary.wiley.com/doi/pdf/10.1029/2022GL100141>, 2022.
- Ritz, C., Edwards, T. L., Durand, G., Payne, A. J., Peyaud, V., and Hindmarsh, R. C. A.: Potential sea-level rise from Antarctic ice-sheet instability constrained by observations (Supplement), *Nature*, <https://doi.org/10.1038/nature16147>, 2015.



- Schannwell, C., Drews, R., Ehlers, T. A., Eisen, O., Mayer, C., Malinen, M., Smith, E. C., and Eisermann, H.: Quantifying the effect of ocean bed properties on ice sheet geometry over 40 000 years with a full-Stokes model, *The Cryosphere*, 14, 3917–3934, <https://doi.org/10.5194/tc-14-3917-2020>, publisher: Copernicus GmbH, 2020.
- 520 Schoof, C.: Ice sheet grounding line dynamics: Steady states, stability, and hysteresis, *Journal of Geophysical Research*, 112, F03S28, <https://doi.org/10.1029/2006JF000664>, 2007.
- Schoof, C.: Marine ice sheet stability, *Journal of Fluid Mechanics*, 698, 62–72, <https://doi.org/10.1017/jfm.2012.43>, publisher: Cambridge University Press, 2012.
- Schwans, E., Parizek, B. R., Alley, R. B., Anandakrishnan, S., and Morlighem, M. M.: Model insights into bed control on retreat of Thwaites
525 Glacier, West Antarctica, *Journal of Glaciology*, pp. 1–19, <https://doi.org/10.1017/jog.2023.13>, publisher: Cambridge University Press, 2023.
- Sergienko, O. V.: No general stability conditions for marine ice-sheet grounding lines in the presence of feedbacks, *Nature Communications*, 13, 2265, <https://doi.org/10.1038/s41467-022-29892-3>, number: 1 Publisher: Nature Publishing Group, 2022.
- Sergienko, O. V. and Wingham, D. J.: Bed topography and marine ice-sheet stability, *Journal of Glaciology*, 68, 124–138,
530 <https://doi.org/10.1017/jog.2021.79>, publisher: Cambridge University Press, 2022.
- Shepherd, A., Fricker, H. A., and Farrell, S. L.: Trends and connections across the Antarctic cryosphere, *Nature*, 558, 223–232, <https://doi.org/10.1038/s41586-018-0171-6>, 2018.
- Still, H., Campbell, A., and Hulbe, C.: Mechanical analysis of pinning points in the Ross Ice Shelf, Antarctica, *Annals of Glaciology*, 60, 32–41, <https://doi.org/10.1017/aog.2018.31>, publisher: Cambridge University Press, 2019.
- 535 Sun, S. and Gudmundsson, G. H.: The speedup of Pine Island Ice Shelf between 2017 and 2020: reevaluating the importance of ice damage, *Journal of Glaciology*, pp. 1–9, <https://doi.org/10.1017/jog.2023.76>, publisher: Cambridge University Press, 2023.
- Surawy-Stepney, T., Hogg, A. E., Cornford, S. L., and Davison, B. J.: Episodic dynamic change linked to damage on the Thwaites Glacier Ice Tongue, *Nature Geoscience*, 16, 37–43, <https://doi.org/10.1038/s41561-022-01097-9>, number: 1 Publisher: Nature Publishing Group, 2023.
- 540 Tinto, K. J. and Bell, R. E.: Progressive unpinning of Thwaites Glacier from newly identified offshore ridge: Constraints from aerogravity, *Geophysical Research Letters*, 38, <https://doi.org/10.1029/2011GL049026>, _eprint: <https://onlinelibrary.wiley.com/doi/pdf/10.1029/2011GL049026>, 2011.
- Wild, C. T., Alley, K. E., Muto, A., Truffer, M., Scambos, T. A., and Pettit, E. C.: Weakening of the pinning point buttressing Thwaites Glacier, West Antarctica, *The Cryosphere*, 16, 397–417, <https://doi.org/10.5194/tc-16-397-2022>, publisher: Copernicus GmbH, 2022.
- 545 Winkelmann, R., Martin, M. A., Haseloff, M., Albrecht, T., Bueler, E., Khroulev, C., and Levermann, A.: The Potsdam Parallel Ice Sheet Model (PISM-PIK) – Part 1: Model description, *The Cryosphere*, 5, 715–726, <https://doi.org/10.5194/tc-5-715-2011>, 2011.

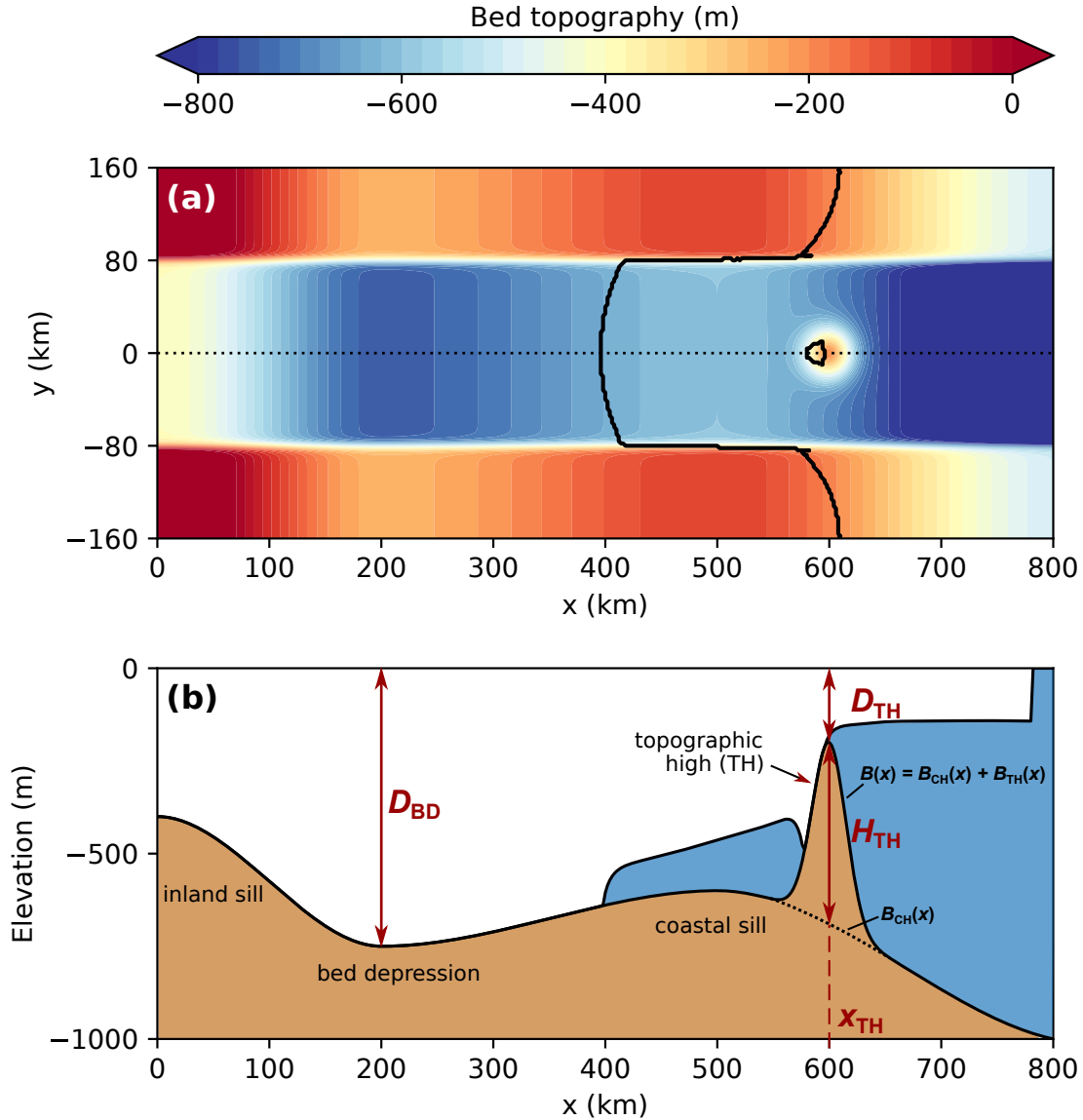


Figure 1. (a) Channel-type bed topography, $B(x, y)$, prescribed in the laterally confined simulations (colorbar) with steady-state GL position of the ice-sheet-shelf system and its pinning point (black contours). (b) Cross section along centerline ($y = 0$, dotted line in panel a) of region below sea level with bed topography (brown), ice body (white) and ocean (blue). The bed profile, $B(x)$ (continuous black contour), results from the superposition of the channel component of the bed topography, $B_{CH}(x)$ (dotted black contour), and the Gaussian-shaped topographic high, $B_{TH}(x)$, of height H_{TH} (see Eqs. 1-3). The parameters varied in the experiments are denoted in red, i.e., the depth of the bed depression, D_{BD} , the depth of the topographic high, D_{TH} , and the location of the topographic high, x_{TH} . Also highlighted are the locations of the topographic high, the inland sill, the bed depression and the coastal sill as referred to in the text. For the example shown here, the parameter values are $D_{BD} = 750$ m, $D_{TH} = 200$ m and $x_{TH} = 600$ km.

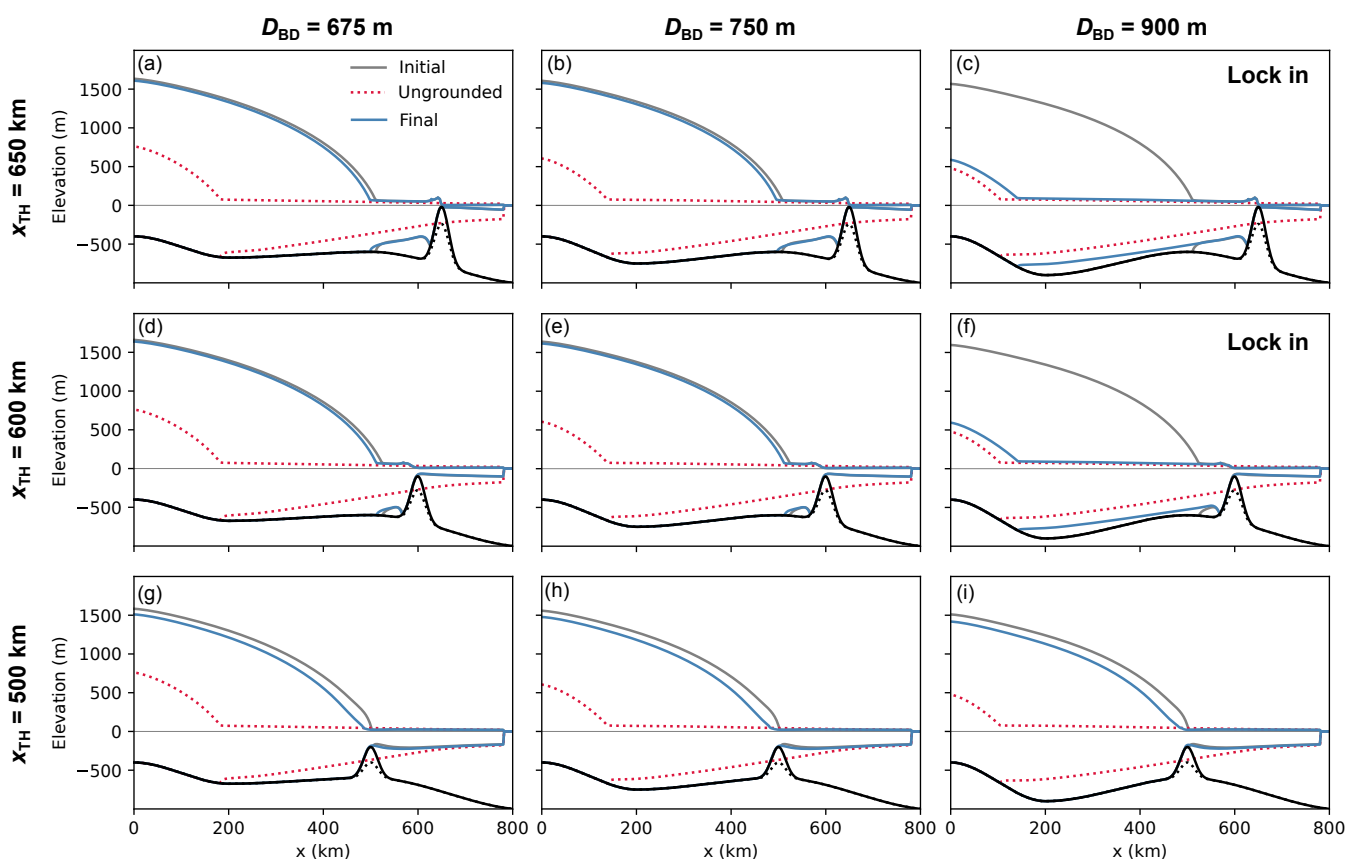


Figure 2. Steady-state centerline profiles for each set of the laterally confined hysteresis experiments, i.e., for each of the nine combinations of bed-depression depth, D_{BD} (columns), and topographic-high location, x_{TH} (rows). Shown are the initial state before perturbation (grey), the state after ice-shelf ungrounding from the topographic high (red dotted) and the final state, i.e., after the topographic high has been raised to its original value (blue). Bed topography in black with the dotted profile showing the topographic high at the stage of ice-shelf ungrounding (associated with red dotted glacier profile). The two sets of hysteresis experiments showing lock-in behavior (the glacier does not revert to its original state) are marked in the upper right corner.

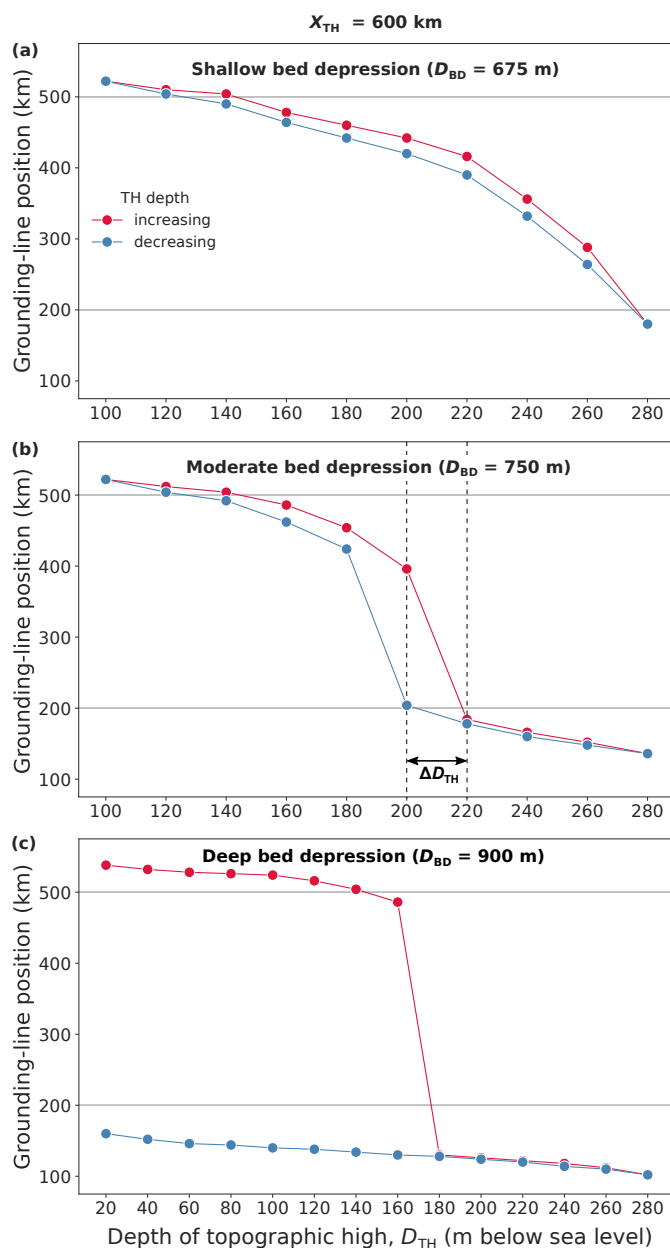


Figure 3. Hysteresis curves of steady-state centerline GL positions in the laterally confined simulations for a step-wise increase (red) and subsequent decrease (blue) of the depth of the topographic high on which the ice shelf is pinned (see Fig. S1 for timeseries of the GL evolution). The topographic high is located at $x_{TH} = 600 \text{ km}$. The panels show results for three different bed-depression depths, **(a)** $D_{BD} = 675 \text{ m}$ (shallow), **(b)** $D_{BD} = 750 \text{ m}$ (moderate) and **(c)** $D_{BD} = 900 \text{ m}$ (deep). The two grey horizontal lines mark the range of the retrograde bed section between the tip of the coastal sill (at $x = 500 \text{ km}$) and the deepest point of the bed depression (at $x = 200 \text{ km}$). The dashed vertical lines in panel b denote the hysteresis gap ΔD_{TH} , quantifying the amount of additional change in forcing required to tip back the glacier from its retreated state towards its advanced state on the path of regrowth (blue curve) compared to the path of retreat (red curve).

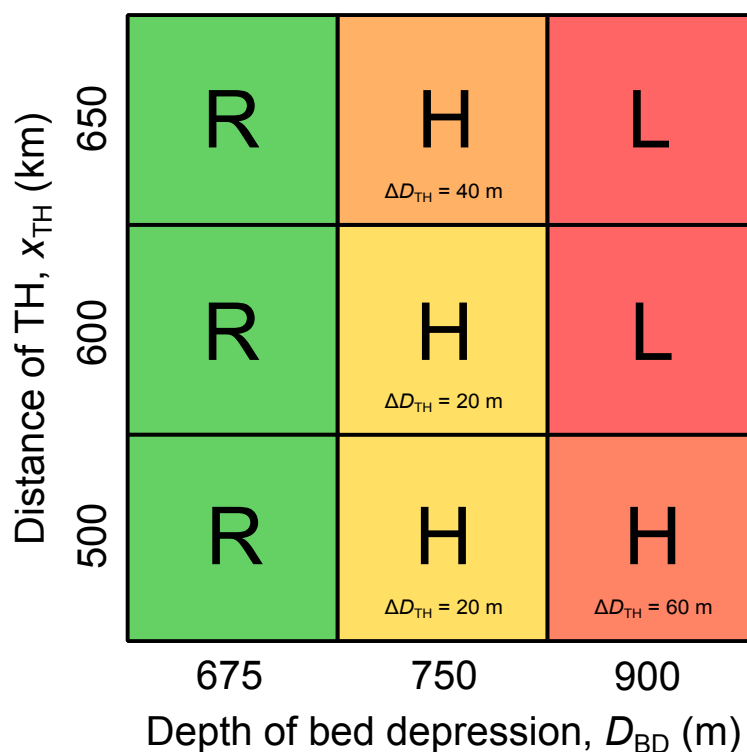


Figure 4. Regime diagram of qualitative glacier response in the laterally confined simulations to the applied lowering and subsequent raising of the topographic high on which the ice shelf is grounded, dependent on the depth of the bed depression below sea level (x axis) and the distance of the topographic high to the ice divide (y axis). Regimes are "R" for reversible glacier retreat and re-advance (green), "H" for hysteretic behavior (yellow to reddish; more reddish for larger hysteresis gap Δh_{TH} between retreat and advance) and "L" for lock in, i.e., no re-advance (red).

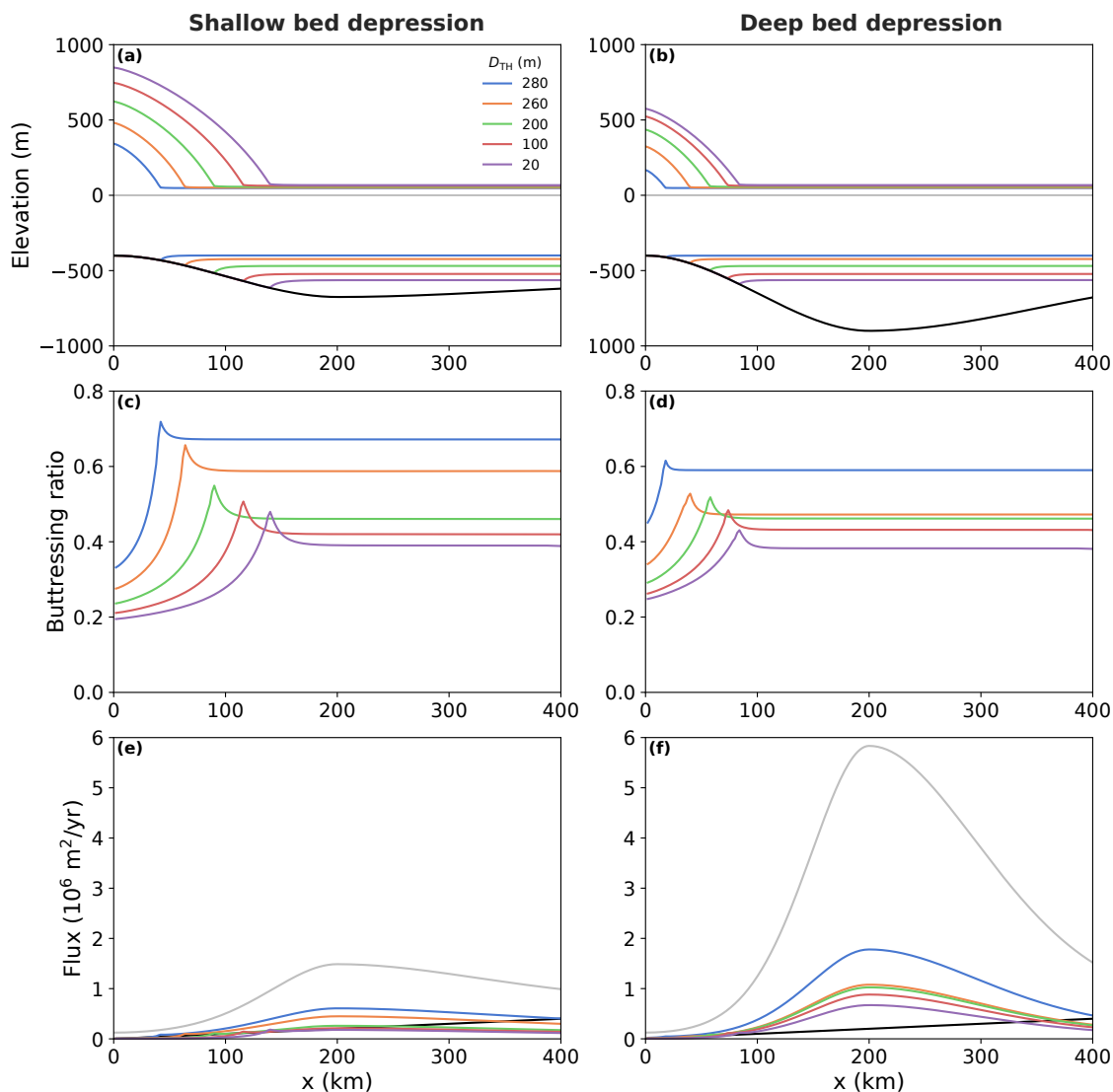


Figure 5. Centerline diagnostics from laterally unconfined simulations of the re-growing ice-sheet-shelf system (decreasing topographic-high depth D_{TH} ; legend) for the cases of a shallow bed depression (left-hand-side column; $D_{BD} = 675$ m) versus a deep bed depression (right-hand-side column; $D_{BD} = 900$ m). (a), (b) Profiles of the ice-sheet-shelf system (colors) and underlying bed topography (black). (c), (d) Buttrressing ratios diagnosed according to Gudmundsson et al. (2023, Eq. 6). (e), (f) GL flux (colors) calculated according to the boundary layer theory by Schoof (2007, Eq. 29), based on the prescribed bed topography and the buttrressing ratio. Integrated surface accumulation rate given by black line. The GL flux profile for the unbuttrressed case is shown in grey.



Table 1. Physical constants and parameter values as prescribed in the laterally confined and laterally unconfined simulations.

Parameter	Value		Unit	Physical meaning
	Laterally confined	Laterally unconfined		
a	0.15	1.0	m yr^{-1}	Surface accumulation rate
A	$3.169 \cdot 10^{-25}$		$\text{Pa}^{-3} \text{s}^{-1}$	Ice softness
C	$3.981 \cdot 10^6$		$\text{Pa m}^{-1/3} \text{s}^{1/3}$	Basal friction parameter, entering Eq. (3) of Cornford et al. (2020)
g	9.81		m s^{-2}	Gravitational acceleration
m	1/3			Basal friction exponent, entering Eq. (3) of Cornford et al. (2020)
n	3			Exponent in Glen's law
ρ_i	918		kg m^{-3}	Density of ice
ρ_o	1028		kg m^{-3}	Density of ocean water
d_c	500	-	m	Depth of bed trough compared with side walls, entering Eq. (1) of Cornford et al. (2020)
f_c	4		km	Characteristic width of bed-trough side walls, entering Eq. (1) of Cornford et al. (2020)
w_c	80	160	km	Half-width of bed trough, entering Eq. (1) of Cornford et al. (2020)
D_{BD}	{675, 750, 900}	{675, 900}	m	Depth of bed depression below sea level
D_{TH}	{20, ..., 400}	{20, ..., 300}	m	Range of topographic-high depths (20-m steps)
L_x	800		km	Length of computational domain (x dimension)
L_y	320	160	km	Width of computational domain (y dimension)
x_{CF}	780		km	Position of fixed calving front
x_{TH}	{500, 600, 650}	600	km	x location of topographic-high center
y_{TH}	0		km	y location of topographic-high center